The origin of the low-velocity anomalies beneath the rootless Atlas Mountains: an insight gained from modeling of anisotropy developed by the travel of Canary Plume

Hwaju Lee[1,2*], Maximilano J. Bezada[1], YoungHee Kim[2]

[1]School of Earth & Environmental Sciences, University of Minnesota, Minneapolis, Minnesota, USA

[2]School of Earth and Environmental Sciences, Seoul National University, Seoul, Republic of Korea

[*]Corresponding author: Hwaju Lee (leex8217@umn.edu)

Hwaju Lee was at the University of Minnesota now at Seoul National University.

Key Points:

- Teleseismic P-wave tomography considering anisotropy is used to study the origin of low-velocity anomalies found below the Moroccan Atlas.
- We incorporate anisotropy as a priori constraint in tomography and show the reduction of low-velocity anomalies below the Moroccan Atlas.
- Lateral travel of plume materials from Canary Hotspot can be a source of low-velocity anomalies.

Abstract

When a mantle plume rises from the deep mantle and reaches the base of a tectonic plate, it changes the traveling direction from vertical to horizontal. The horizontal spread of plume material is often radially asymmetric. The plume found below the Canary Hotspot is an example. Previous studies have suggested that the channeling of the Canary Plume toward the westernmost Mediterranean (Alboran Sea) may have contributed to the high elevation of the Moroccan Atlas Mountains while regional upwelling and edge-driven convection are proposed as other candidates to explain the topography. Since mantle flow can develop seismic anisotropy, in this study we incorporate anisotropy as a priori constraint in teleseismic P-wave tomography. Our improved tomography result favors the hypothesis that the lateral travel of Canary Plume material supports the isostatically unstable Moroccan Atlas.

Plain Language Summary

The propagation velocity of seismic waves is sensitive to temperature. Low seismic velocities in the mantle found from seismic tomography, a technique to image the velocity structure of inner Earth with seismic waves, are commonly interpreted as high-temperature or hydrous regions in the mantle. As a result, seismic tomography has been the primary tool for revealing mantle structures such as hot plumes rooted in the deep mantle that play significant roles in the mantle dynamics. Previous studies have shown that the risen plume materials can drag the surrounding mantle and consequently cause directional dependence of the seismic velocities, which also affects the results of the seismic tomography in addition to temperature and hydrous conditions. This study improves the quality of seismic tomography results by considering such directional dependence of wave speeds in the mantle in order to elucidate the evolution of the mantle plume and its interaction with the upper plate in Morocco. The imaged low-velocity conduit below the high-altitude Moroccan Atlas indicates lateral travel of the mantle plume originated from the Canary Hotspot in northwest Africa, which may have dragged the surrounding mantle beneath the Moroccan Atlas.

1. Introduction

Since Wilson (1963) suggested the existence of mantle plumes to explain the Hawaiian island chain, the vertical rise of the buoyant mantle from the deep mantle and consequent decompression melting near the surface have been considered a mechanism of hotspots (e.g., Morgan, 1971; Sleep, 1990). The buoyancy of the hot mantle primarily comes from the temperature, and, therefore, there have been many attempts to better constrain the mantle plume structure using seismic tomography as the high-

temperature mantle is imaged as low-seismic-velocity anomalies (e.g., DePaolo & Manga, 2003; French & Romanowicz, 2015; Humphreys et al., 2000; Montelli et al., 2006; Nolet et al., 2007; Ritter et al., 2001; Zhao, 2007). When the plume reaches the base of a plate, it has to deflect its direction of travel from vertical to sub-horizontal. However, the horizontal spread of the plume is not always radially symmetric. Instead, previous studies have suggested that the plume material can be dragged by or can drag the direction of the surrounding mantle flow (e.g., Ito et al., 2014; Ribe & Christensen, 1994, 1999; Richards & Griffiths, 1988; Sleep, 1990; Thoraval et al., 2006). Consequently, this lateral travel of mantle plume can extend hundreds to thousands of kilometers while accommodating magmatism and the development of (sea) mountain systems on the upper plate. For instance, it has been proposed based on geophysical and geochemical data that the Afar and Réunion hot plumes are horizontally (or laterally) channeling beneath Arabia (e.g., Bagley & Nyblade, 2013; Chang & Van der Lee, 2011; Hansen et al., 2012) and the western Indian Ocean (e.g., Barruol et al., 2019; Füri et al., 2011; Morgan, 1978; Sleep, 2008), respectively. The lateral travel of the mantle plume from the Juan Fernández hotspot has been suggested to explain low-velocity anomalies found below the Nazca Plate in Chile (e.g., Portner et al., 2017). The lateral channeling of the plume from the Canary Hotspot Islands (28°N, 16°W) toward the westernmost Mediterranean (i.e. Alboran Sea) has been also suggested as an origin of the low-velocity anomalies beneath Morocco (Duggen et al., 2009; Miller et al., 2015) while other scenarios such as edge-driven-convection and delamination-initiated local upwelling have alternatively been suggested as their origin (Kaislaniemi & van Hunen, 2014; Missenard et al., 2006; Missenard & Cadoux, 2012). Utilizing teleseismic P-wave tomography, this study serves as a case study that examines various scenarios including the lateral channeling of Canary Plume while exploring a detailed deep mantle structure of the High and Middle Atlas Mountains based on seismic anisotropy developed by the evolution of mantle flow.

1.1. Tectonic Framework of the Moroccan Atlas and Its Deep Structure

The High and Middle Atlas Mountains (hereinafter, Moroccan Atlas or the Atlas Mountains) are an intra-continental mountain range that extends from the Atlantic coast of southwest Morocco to the northeastern border between Morocco and Algeria (Figure 1a). Although it is not at a convergent boundary, the Atlas mountain ranges are one of the highest mountains in Africa. The mountains formed as a result of the inversion of Triassic-Jurassic age grabens when Africa converged with Eurasia during the Cenozoic (Arboleya et al., 2004; Brede et al., 1992; Gomez et al., 1998; Piqué et al., 2002; Teixell et al., 2003). However, the estimated tectonic shortening due to the compression during the Eocene and Pliocene-Quaternary is not enough to support the topography of the Atlas (Beauchamp et al., 1999; Frizon

de Lamotte et al., 2000; Gomez et al., 1998; Teixell et al., 2003, 2009). Previous studies suggested no deep crustal root (Ayarza et al., 2005; Miller & Becker, 2014; Missenard et al., 2006; Sandvol et al., 1998) and thinned lithosphere beneath the mountains (Anahnah et al., 2011; Ayarza et al., 2005; Miller & Becker, 2014; Missenard et al., 2006; Sun et al., 2014; Teixell et al., 2003, 2005; Timoulali et al., 2019; Zeyen et al., 2005). Detailed geophysical investigations further found a conduit of the low-velocity anomalies below the mountains (Bezada et al., 2014; Calvert et al., 2000; Fullea et al., 2010; Miller et al., 2015; Palomeras et al., 2014; Seber et al., 1996; Timoulali et al., 2015). These investigations conclusively interpret that the buoyancy, which comes from the hot mantle, is supporting the high topography of the mountains instead of a crustal root. The presence of a hot mantle is consistent with the intra-plate alkali Cenozoic magmatism in Morocco (Figure 1b) (Anguita & Hernán, 2000; Lustrino & Wilson, 2007; Teixell et al., 2005). The first volcanic activity took place 40 – 67 Ma (Figure 1b, yellow triangles), and the second volcanic activity, which is much more voluminous, took place ~30 Ma (Figure 1b, red triangles).

To explain the loss of mantle lithosphere and the origin of the hot mantle, lithospheric delamination has been proposed, but what initiated the delamination has not met a consensus yet between a few hypotheses (Table 1): 1) crustal thickening and consequent mantle upwelling after the delamination (Ebinger & Sleep, 1998; Fullea et al., 2010; Lustrino & Wilson, 2007; Ramdani, 1998), 2) development of small-scale edge-driven convection (EDC) in the mantle between the West-African Craton and Atlas lithosphere (Kaislaniemi & van Hunen, 2014; Missenard & Cadoux, 2012), and 3) travel of Canary mantle plume (28°N, 16°W), which may have removed the base of the lithosphere below the Atlas (Anguita & Hernán, 2000; Duggen et al., 2009; Miller et al., 2015; Miller & Becker, 2014; Sun et al., 2014). The travel of Canary Plume material toward the Alboran Sea and consequent lithospheric delamination is more consistent with the geochemical analysis (Anguita & Hernán, 2000; Duggen et al., 2009) and shear-wave splitting (SWS) observation (Buontempo et al., 2008; Diaz et al., 2010; Miller et al., 2013; Miller & Becker, 2014). The geochemical analysis of mafic lavas from the Middle Atlas showed that it shares similar geochemical properties with ones from the Canary Islands (Anguita & Hernán, 2000; Duggen et al., 2009). Duggen et al. (2009) further suggested the mantle suction due to the rollback of the Alboran slab found below the Alboran Sea (the westernmost Mediterranean) may have become a driving force for the lateral travel of mantle plume. Meanwhile, based on waveform modeling, Sun et al. (2014) suggested a possible presence of the low-velocity column beneath the Middle Atlas, and Miller et al. (2015) suggested that the uprising plume conduit has been branched out based on results from receiver function analysis.

1.2. Seismic Anisotropy evidenced by SWS observations

The observation of SWS based on dense seismic coverage in Morocco and its vicinity is an inevitable piece of evidence of seismic anisotropy in the region (Buontempo et al., 2008; Diaz et al., 2010; Miller et al., 2013; Miller & Becker, 2014). The observed delay time (dt) is < 1 second in the High Atlas and it gradually increases to ~2 seconds in NE Morocco. The observed fast polarization direction (FPD) of the Middle Atlas and High Atlas is generally oriented in the NE direction (Figure 1b) (Diaz et al., 2010, 2015; Miller et al., 2013). The predominant source of seismic anisotropy inferred from the SWS data is the lattice preferred orientation (LPO) of olivine in the mantle rock. Since mantle flow can develop LPO, investigating seismic anisotropy provides a useful insight into the orientation of mantle flow (e.g., Christensen, 1984; Fouch & Rondenay, 2006; Ismaïl & Mainprice, 1998; Silver, 1996).

At the same time, seismic anisotropy can influence seismic travel times and be consequently imaged as velocity anomalies (e.g., Bezada et al., 2016; Blackman Donna K. & Kendall J.-Michael, 1997; Eberhart-Phillips & Mark Henderson, 2004; Ishise & Oda, 2005; Lloyd & Van der Lee, 2008; Wu & Lees, 1999). When mantle rocks experience shear stress, the seismically fast direction (SFD) (i.e., a-axis) of A-type olivine aligns subparallel to the direction of maximum shear (i.e., the direction of mantle flow) (e.g., Anderson, 1989; Hirth & Kohlstedt, 2003; Ismaïl & Mainprice, 1998; Kaminski & Ribe, 2002; Tommasi et al., 1999). As a result, assuming a simplified hexagonal symmetry for olivine anisotropy, the mantle with SFD aligned subparallel to the surface (or plate) (i.e., aligned perpendicular to the traveling direction of teleseismic rays) can be imaged as low-velocity anomalies. Conversely, the mantle with SFD aligned perpendicular to the surface (or plate) (i.e., aligned parallel to the traveling direction of teleseismic rays) can be imaged as high-velocity anomalies. For sub-horizontal orientations of LPO, seismic anisotropy can be mapped in isotropic tomography as low-velocity anomalies, in addition to the warmer and hydrous mantle (e.g., Faccenda & Capitanio, 2012; Hu et al., 2017; Kaminski & Ribe, 2002; Lee et al., 2021).

Thus, given the observations of SWS, we attempt to decipher the current mantle configuration by taking advantage of the LPO of A-type olivine developed by mantle flow. As different configurations of mantle flow are expected by various tectonic scenarios suggested for the region, exploring seismic anisotropy may shed light on how mantle flow is configured currently and where the low-velocity anomalies beneath the Atlas Mountains and NE Morocco come from. Furthermore, we try to examine the contribution of seismic anisotropy to the P-wave low-velocity anomalies found beneath Morocco (Figure 1c) that have been interpreted as mantle materials with a possibly excessive temperature or partial melt regardless of suggested origins.

2. Data, Method, and Anisotropy Models

2.1. Data and Method

We use the tomographic inversion method of Bezada et al. (2014) and the data of 76,524 delays from 332 events recorded by 398 stations in the Iberian Peninsula and Morocco (triangles of Figure 1b and Figure S1). After we obtain the reference arrivals based on the AK135 velocity model (Kennett et al., 1995), we determine the delay times from cross-correlation (VanDecar & Crosson, 1990) in three different frequency bands (0.3, 0.5, and 1.0 Hz). These delays are inverted for the tomographic inversion using the hybrid ray-tracing method, introduced by Bezada et al. (2013), which combines iterative ray tracing and finite-frequency kernels. The ray-tracing inside the velocity model is carried out by accounting for 3D structure using a method based on graph theory (Hammond & Toomey, 2003; Toomey et al., 1994), and outside of the modeled volume is 1D. For depths above ~80 km, we implement the surface wave tomography model of Palomeras et al. (2014) as a starting model.

To incorporate seismic anisotropy in the tomographic inversion, we include a hypothetical anisotropy model as an *a priori* constraint instead of inverting for anisotropy in the tomographic model (i.e., full anisotropic inversion). For each iteration, we calculate travel times through the previous isotropic velocity model with the chosen anisotropy and subtract these values from the observations. This assumes that the delay times imposed by the hypothetical seismic anisotropy model have been removed from the observed delays and so the new set of delay times is considered as purely coming from the isotropic structure, which allows us to carry the isotropic inversion. Using synthetic and real data, Bezada et al. (2016) and Lee et al. (2021) have shown that this approach is a functional alternative to the full anisotropic inversion. We expect a reduction in model norm and delay time misfit if our anisotropy model is a good approximation of the true anisotropy field in the mantle (Bezada et al., 2016).

2.2. Anisotropy Models

We accommodate various scenarios as the source for the thinned lithosphere beneath the Moroccan Atlas into five different anisotropy models (Table 1): Upwelling (UpW) (Ebinger & Sleep, 1998; Fullea et al., 2010; Lustrino & Wilson, 2007; Ramdani, 1998), Edge-drive convection (EDC) (Kaislaniemi & van Hunen, 2014; Missenard & Cadoux, 2012), Lateral conduit (Lateral) (Anguita & Hernán, 2000; Duggen et al., 2009; Miller & Becker, 2014), OneStem (one upwelling stem of the lateral conduit of Canary Plume below the Middle Atlas) (Sun et al., 2014), and TwoStems (two upwelling stems below the Middle Atlas and northeast (NE) Morocco, respectively) (Miller et al., 2015).

Table 1. Description of anisotropy models

Source of the thinned lithosphere	Crustal thickening	Edge-driven convection	Travel of Canary Plume		
Model name	**UpW**	**EDC**	**Lateral**	Plume branches	
				OneStem	**TwoStems**
Spatial and depth distributions	The distribution of low-velocity anomalies at 60 – 160 km			The distribution of low-velocity anomalies at 60 – 160 km with upwelling stem at 160 – 200 km	
Anisotropy field	To reproduce 1 second of delay time				
Consistency with the observed SWS	x	x	√	√	√

2.2.1. Spatial and Depth distribution

All of our anisotropy models are based on the spatial and depth distributions of the low-velocity anomalies found from the result of isotropic tomography (Figure 1c and Figure S2). To explore the contribution of seismic anisotropy to the low-velocity anomalies in Morocco, we hypothetically assume that the low-velocity anomalies, which are slower than 2% P-wave velocity perturbation (dVp/Vp) below the Moroccan Atlas and NE Morocco, solely come from the seismic anisotropy (Figure 1c and Figure S2). As we find such low-velocity anomalies at 60 – 160 km depth, we assume that seismic anisotropy is predominantly distributed at 60 – 160 km depth (Figure S2), except for anisotropy models OneStem and TwoStems. Anisotropy model OneStem has a stem portion representing the uprising hot mantle column beneath the Middle Atlas (Sun et al., 2014) while model TwoStems has an additional stem beneath NE Morocco (Miller et al., 2015) (Figure 2 and Figure S3). The stems are at 160 – 200 km depth and are represented by cylindrical columns with 100 km diameters specifically centered at station PM22 (33.30°N, 5.11°W) for both OneStem and TwoStems for the Middle Atlas region while TwoStems have another stem centered at station PM39 (34.89°N, 2.61°W) for and NE Morocco (i.e., the only difference between OneStem and TwoStems is that TwoStems have one more stem centered at station PM39 in the NE Morocco region) (Figure 2).

2.2.2. Anisotropy field

The magnitude of anisotropy in the models is uniform and homogeneous for all anisotropy models and it is estimated to reproduce the observed 1.0-second delay time, which is the mean of observed delay time within the study area, from 60 – 160 km depth for a vertically

incident S wave (black-dashed box in Figure 1c) (Diaz et al., 2010, 2015; Miller et al., 2013) except for the stems of the anisotropy model OneStem and TwoStems. As stems extend to 200 km depth, the stem portions are set to reproduce a 1.0-second delay from 60 – 200 km depth. To convert the observed SWS time into the anisotropy model for P-wave tomography, we multiply a factor of 1.51 by S-wave velocity anisotropy (AVs) to obtain P-wave velocity anisotropy (AVp) (i.e., AVp/AVs = 1.51) based on elastic tensors of natural peridotite sample (Hammond & Toomey, 2003; Kern, 1993) and the estimated magnitude of anisotropy is 6.7% while it is 4.8% for the stem portions of OneStem and TwoStems.

2.2.3. Consistency with observed SWS

Seismic anisotropy can be mapped as velocity anomalies in isotropic tomography depending on the orientation of SFD of A-type olivine. As we expect SFD to be vertically aligned (i.e., parallel to the ray path) when the mantle is upwelling, we implement the SFD to be vertically aligned for the anisotropy model UpW and upwelling portion of the EDC as well as for the stems of the OneStem and TwoStems models (Figure 2 and Figure S3). For the horizontally circulating portion of EDC, the SFD is aligned at -45° to the north approximately considering the location of the North African cratonic edge as previous studies have suggested (Kaislaniemi & van Hunen, 2014; Missenard & Cadoux, 2012). For the SFD of the anisotropy model Lateral as well as the non-stem portion of OneStem and TwoStems, we interpolate the observed FPD of SWS into a fine grid to reflect the change of FPD (Figure 1b) assuming all of the SFD are aligned parallel to the surface.

3. Results

3.1. Residual Time and Model Norm

We find insignificant changes in the residual time when we consider different anisotropy models compared to the isotropy model (denoted as Isotropy) (Table 2). For the Moroccan Atlas and NE Morocco (31.0° – 35.5° latitude, -8.0° – -1.5° longitude; black-dashed box in Figure 1c), the residual time of the isotropic velocity model is 0.245 seconds while it is 0.253, 0.258, 0.247, 0.248, and 0.249 seconds for UpW, EDC, Lateral, OneStem, and TwoStems, respectively. Although the changes are very small, the residual time of EDC is increased most (by ~5%) compared to that of the Isotropy case.

Meanwhile, we find moderate changes in the model norm within the study area at 60 – 200 km depth. We note that the anisotropy models UpW, EDC, and Lateral are placed at depths of 60 – 160 km,

but we compare the model norm within 60 – 200 km depth for the study region (31.0° – 35.5° latitude, -8.0° – -1.5° longitude; black-dashed box in Figure 1c) as the stems of OneStem and TwoStems extend to 200 km depth. We find a reduction of the model norm from including anisotropy model Lateral (0.463), OneStem (0.498), TwoStems (0.503) compared to the model norm of Isotropy (0.560) (Table 2). In contrast, we find an increase in the model norm from UpW (0.765) and EDC (0.617). As a result, compared to Isotropy, the model norm of UpW has increased by ~35% while Lateral has decreased the most, by ~15%.

Table 2. Results of the isotropy and five different anisotropy models

Model Name	Isotropy	UpW	EDC	Lateral	OneStem	TwoStems
RMS Residual Time (s)	**0.245**	0.253	0.258	0.247	0.248	0.249
Model Norm	0.560	0.765	0.617	**0.463**	0.498	0.503
MSAT Misfit (s)	1.098	1.098	1.103	**0.678**	0.691	0.721

3.2. P-wave Tomography

For the High Atlas, we observe insignificant changes in the low-velocity anomalies between the isotropic and anisotropic tomographies except for UpW ('H' in Figure 3g – l). The High Atlas region of UpW the model shows an increase in low-velocity anomalies by ~0.5 dVp/Vp %.

In the Middle Atlas region, compared to the model Isotropy, we also find minor changes in the low-velocity anomalies for the shallower depth (< 90 km) except for UpW, which shows an increase in low-velocity anomalies by ~0.5% ('M' in Figure 3g – l). For the deeper depths (i.e., 90 – 160 km), models Lateral and EDC show a ~2% reduction in the low-velocity anomalies while UpW shows more than a 1.5% increase in the low-velocity anomalies (Figure 3 and Figure S4). However, model EDC shows a dramatic increase in the low-velocity anomalies in the northern region of the Middle Atlas where model EDC has SFD aligned vertically reflecting the upwelling portion of mantle convection (Figure2, Figure 3c, Figure S3, and Figure S4). In the deeper depth below the Middle Atlas region, we observe a blob of a high-velocity anomaly at depth of 300 – 400 km from both the isotropic and anisotropic models ('D' in Figure 3g – l).

Among the three regions of High Atlas, Middle Atlas, and NE Morocco, we observe the most significant changes below the NE Morocco region (Figure 3 and Figure S4). For all models except for the UpW and deeper depth of TwoStems (i.e., 125 – 200 km depth), we find a decrease in the low-velocity anomalies. Among the anisotropic models that show the decrease in the low-velocity anomalies, model

Lateral shows the most reduction of up to ~2% in the low-velocity anomalies from 90 km to the deeper depth. Model EDC shows a similar reduction above 90 km to Lateral, but reduction becomes ~1% below 90 km depth which is similar to the reduction of OneStem. Model UpW and TwoStems, which has an extra stem portion in NE Morocco in comparison to OneStem, present an extension of the low-velocity column to a depth of ~300 km while this low-velocity column is greatly reduced in EDC, Lateral, and OneStem compared to the isotropic model (Figure 2 and Figure 3).

3.3. Predicted SWS

To predict the SWS produced by the anisotropy models, we utilize the Matlab Seismic Anisotropy Toolbox (MSAT) (Walker & Wookey, 2012) (see details in Lee et al. (2021)) (Figure 4 and Figure 5). We measure the vector difference between observed and predicted SWS as a misfit. As null splitting is expected when SFD is aligned parallel to the ray path (i.e., vertically aligned SFD to the surface), we find no splitting from the Isotropy and UpW as well as the upwelling portion of EDC. The MSAT misfits for both Isotropy and UpW are 1.098 seconds while EDC has the largest misfit of 1.103 seconds (Table 2). We find the best misfit from Lateral, 0.678 seconds followed by OneStem (0.691 s) and TwoStems (0.721 s). As the stem portions of OneStem and TwoStems have the SFD aligned vertically (darker gray circles in Figure 4), the splitting above the stem regions is smaller than for model Lateral and this leads the misfit to be larger than in the same locations for model Lateral.

4. Discussion

4.1. Analysis of residual time, model norm, and SWS misfit

From the results of residual time, model norm, and SWS misfit of the Isotropy model and five different anisotropic models, we find that model Lateral can be considered the best among the anisotropy models. As shown in Bezada et al. (2016), a good approximation of anisotropy structure in tomographic inversion will result in reductions in the travel time residuals and model norm. From all of the anisotropy models, we find insignificant changes (< 5%) in travel time residuals compared to Isotropy. Among the anisotropic models, we find the closest time residuals from Lateral (0.247 s) to Isotropy (0.245 s) followed by OneStem (0.248 s) and TwoStems (0.249) (Table 2 and Figure 5) while we find the most increased residuals from model EDC (0.258 s). In terms of the model norm, including model Lateral reduces the model norm the most, by over 15%, compared to Isotropy. We still find a reduction in model norm from One Stem (0.498 and ~10%) and TwoStems (0.503 and ~10%). In contrast, we find the largest increase from UpW (0.765), by ~37%, followed by EDC (0.617), which shows a ~10% increase. The

misfit result between observed and predicted SWS is consistent with the change in residual time and model norm: the misfit of SWS from Lateral (0.678 s) is about 40% smaller than Isotropy (1.098 s). Having upwelling stems beneath the Middle Atlas (i.e., OneStem, 0.691 s) and NE Morocco (i.e. TwoStems, 0.721 s) produces larger misfits than Lateral, which has no upwelling-associated SFD in the model. Jointly considering the changes in the three metrics of residual time, model norm, and SWS misfit, we find that the model Lateral is the best approximation of anisotropic structure among the five anisotropy models. We note, however, that we find a slightly larger model norm and SWS misfit while the residual time is only marginally different from OneStem compared to the result of Lateral. It also suggests that model OneStem may also be a good approximation of anisotropy structure in the study region. At the same time, our results strongly suggest that UpW and EDC are not good approximations of anisotropy structure in the region, as none of the three metrics are improved over the model Isotropy. Consequently, as Lateral represents the lateral travel of the Canary plume while OneStem comes with one branch, we learn that the current configuration of the mantle is most consistent with the travel of the Canary plume as a source of low-velocity anomalies found beneath Morocco (Figure 7).

4.2. Origin of the low-velocity anomalies

Our results show that the higher reductions in the residual time, model norm, and SWS misfit, are accompanied by the reduction in the low-velocity anomalies beneath the Middle Atlas and NE Morocco; specifically at depths greater than 90 km (Figure 6, Figure S4, and Figure S5). The reduction in the low-velocity anomalies is only observed from the anisotropy models whose SFD are aligned subparallel to the surface (i.e. Lateral, horizontally convection portion of EDC, and OneStem beneath NE Morocco), not from ones whose SFD are aligned perpendicular to the surface (i.e., UpW, vertical convection portion of EDC, the stem locations of OneStem and TwoStems). Compatible with the results from the three metrics (section 4.1.) this may imply that the mantle flow is currently configured parallel to the surface (or plate) in the region. In other words, our results favor anisotropy in the mantle that may have developed by the lateral travel of the Canary Plume traveling toward the Alboran Sea (Anguita & Hernán, 2000; Duggen et al., 2009; Miller et al., 2015; Miller & Becker, 2014; Sun et al., 2014) instead of the regional or local upwelling after lithospheric delamination (Ebinger & Sleep, 1998; Fullea et al., 2010; Kaislaniemi & van Hunen, 2014; Lustrino & Wilson, 2007; Missenard & Cadoux, 2012). In addition, the undisturbed low-velocity anomalies below the High Atlas and shallower depths (< 90 km) of the Middle Atlas and NE Morocco regardless of incorporating anisotropy suggest that these anomalies may not solely be a product of seismic anisotropy. This may indicate that the imaged low-velocity anomalies come from other sources of seismically slow mantle conditions such as high temperature and hydrous mantle (Figure 7).

4.3. High-velocity structure in the deeper depth beneath the Middle Atlas

When we compare the isotropic and five anisotropic results, we find unchanged high-velocity anomalies below the Middle Atlas at 300 – 400 km depth (denoted as 'D' in Figure 3g – l). Similar to the unchanged low-velocity anomalies in the shallow depth, we consider that this is not an artifact of unconsidered anisotropy, but rather a true high-velocity structure. Bezada et al. (2014) has shown the same high-velocity structure and it has been interpreted as the delaminated lithosphere. As our results indicate that mantle upwelling is a less favorable scenario in the study region, we are more convinced that the travel of the Canary plume may have initiated the lithospheric delamination. However, unfortunately, it is difficult to conclusively determine the source of delamination and, therefore, further studies on the blob of high-velocity anomalies and their origin will be helpful.

4.4. Origin of the complex SWS in NE Morocco

Unlike the Moroccan Atlas regions, the observed SWS times in the area increase to be ~ 2 seconds, and FPD is irregular and not consistent with the suggested direction of mantle flow in NE Morocco. The change in observed SWS compared to the Moroccan Atlas region may be related more to the location of the Alboran slab below the Alboran Sea (the high-velocity anomalies found below the Alboran Sea in Figure 1c, Figure 3a – f, Figure S4, and Figure S5) (e.g., Bezada et al., 2014; Calvert et al., 2000; Diaz et al., 2010; Miller et al., 2015) and the toroidal mantle flow due to the slab rollback (e.g., Alvarez, 1982; Ayarza et al., 2005; Bezada et al., 2016; Civello & Margheriti, 2004; Faccenda & Capitanio, 2012; Hu et al., 2017; Long & Becker, 2010; Lee et al., 2021; Long & Silver, 2008; Russo & Silver, 1994). Based on our study, it is difficult to separately quantify how much anisotropy is developed by the lateral travel of the Canary plume or rollback of the Alboran slab. Also, despite the facts that 1) it has been suggested that the subduction of the Alboran slab and its retreat/rollback may have created suction of the surrounding mantle (e.g., Duggen et al., 2009; Faccenna et al., 2005) and 2) the moving direction is well aligned with the absolute mantle flow direction suggested by the global model of Conrad & Behn (2010), which predicts NE-SW-directed mantle flow in the study region, exploring the driving mechanism for the extensive distance (~1500 km) for plume travel is beyond the scope of our study.

4.5. Role of seismic anisotropy in tomography for temperature interpretations

To explore the influence of seismic anisotropy on interpretations of mantle conditions below the Moroccan Atlas and NE Morocco, we estimate the temperature of the mantle from the velocity anomalies based on the temperature derivatives with Vp of Cammarano et al. (2003). We choose model Lateral to compare with Isotropy as our results suggest that it is the best approximation to the true anisotropy

structure in the region among the anisotropy models tested (Figure S5). To keep the pressure to be constant at 4 GPa approximately, we choose the 125-km-depth-slice of our velocity model, in which the change of velocity anomalies is significant between the isotropic and anisotropic tomographies (Figure 3 and Figure 6). For this depth, the approximate dry solidus of peridotite is ~1570 °C (Hirschmann, 2000) while the solidus of 5-bulk-wt-% hydrous peridotite is ~1400 °C (Katz et al., 2003). We also assume that the ambient temperature of the mantle at this depth is ~1300 °C based on the study of MORB (Herzberg et al., 2007). At 125 km depth below the High Atlas, the estimated temperature is 1300 – 1500 °C (Figure 6) for both Isotropy and Lateral. This implies that melt is possibly present depending on the water content of the mantle in this depth. For the Middle Atlas, the estimated temperature of the isotropic velocity anomalies is up to ~200 °C above the dry solidus of peridotite. In contrast, the estimated temperature considering seismic anisotropy is below the dry solidus of peridotite. Similar to the High Atlas, the presence of melt is possible depending on the water content of the mantle, but it does not need to be present. For NE Morocco, we find a temperature of ~ 1530 °C from the isotropic model while it is ~ 1350 °C from the anisotropic model. In other words, the presence of melt is not necessary for the anisotropic model below NE Morocco. In summary, for the isotropic model, the presence of melt is necessary for the Middle Atlas regardless of the water content of the mantle; in contrast, when anisotropy is considered, the presence of melt is possible in all regions depending on the hydration condition of the mantle. Relatively high temperatures below both the High and the Middle Atlas can be related to the recent voluminous magmatism during 1.8 – 0.5 Ma (Anguita & Hernán, 2000; Duggen et al., 2009; Teixell et al., 2005). But, further studies will be needed to understand better the relationships between the mantle temperature derived from velocity perturbation and the previous volcanic activities in High Atlas, Middle Atlas, and NE Morocco.

5. Conclusions

Although previous studies have suggested various possible origins for the low-velocity anomalies supporting the rootless Atlas Mountains in Morocco, a consensus has not yet been reached. Mantle flow can develop seismic anisotropy and it is observed by shear wave splitting, which has been studied in the region. Therefore, in this study, by incorporating five representative anisotropy structures in the P-wave teleseismic tomography, we attempt to examine the current configuration of the mantle to help us infer the tectonic evolution and the origin of the low-velocity anomalies. When we include seismic anisotropy as an *a priori* constraint in the tomography, we find the best result in residual time, model norm, and SWS misfit from the anisotropy model reflecting the lateral travel of the Canary plume. In contrast, we

find the least favorable results by including an anisotropy model representing a local upwelling. Simultaneously, we observe that the low-velocity anomalies in the isotropic model are partially produced by unaccounted-for seismic anisotropy beneath the Middle Atlas as well as NE Morocco, which may mislead interpretations of current conditions in the mantle.

Acknowledgments

H. Lee acknowledges the support from the National Research Foundation of Korea (NRF 2021R1A6A3A01086736) and Y. Kim acknowledges support from the Creative Pioneering Researchers Program of Seoul National University (SNU SRnD 3345-20160014). Also, we would like to thank Joseph Byrnes and Hyunsun Kang for the extensive discussion and comments.

Data Availability Statement

Data used in this study are accessible through Incorporated Research Institutions for Seismology (IRIS), Kennett et al. (1995), Diaz et al. (2010), Miller et al. (2013), Bezada et al. (2013), and Palomeras et al. (2014). MATLAB Seismic Anisotropy Toolkit (MSAT) is available through Walker and Wookey (2012).

Reference

Alvarez, W. (1982). Geological evidence for the geographical pattern of mantle return flow and the driving mechanism of plate tectonics. *Journal of Geophysical Research: Solid Earth*, *87*(B8), 6697–6710. https://doi.org/10.1029/JB087iB08p06697

Anahnah, F., Galindo-Zaldívar, J., Chalouan, A., Pedrera, A., Ruano, P., Pous, J., Heise, W., Ruiz-Constan, A., Benmakhlouf, M., López-Garrido, A. C., Ahmamou, M., Galdeano, C. S. de, Arzate, J., Ibarra, P., González-Castillo, L., Bouregba, N., Corbo, F., & Asensio, E. (2011). Deep resistivity cross section of the intraplate Atlas Mountains (NW Africa): New evidence of anomalous mantle and related Quaternary volcanism. *Tectonics*, *30*(5). https://doi.org/10.1029/2010TC002859

Anderson, D. L. (1989). *Theory of the Earth*. , MA Blackwell Scientific Publications.

Anguita, F., & Hernán, F. (2000). The Canary Islands origin: A unifying model. *Journal of Volcanology and Geothermal Research*, *103*(1), 1–26. https://doi.org/10.1016/S0377-0273(00)00195-5

Arboleya, M. L., Teixell, A., Charroud, M., & Julivert, M. (2004). A structural transect through the High and Middle Atlas of Morocco. *Journal of African Earth Sciences*, *39*(3), 319–327. https://doi.org/10.1016/j.jafrearsci.2004.07.036

Ayarza, P., Alvarez-Lobato, F., Teixell, A., Arboleya, M. L., Tesón, E., Julivert, M., & Charroud, M. (2005). Crustal structure under the central High Atlas Mountains (Morocco) from geological and gravity data. *Tectonophysics*, *400*(1), 67–84. https://doi.org/10.1016/j.tecto.2005.02.009

Bagley, B., & Nyblade, A. A. (2013). Seismic anisotropy in eastern Africa, mantle flow, and the African superplume: SEISMIC ANISOTROPY IN EASTERN AFRICA. *Geophysical Research Letters*, *40*(8), 1500–1505. https://doi.org/10.1002/grl.50315

Barruol, G., Sigloch, K., Scholz, J.-R., Mazzullo, A., Stutzmann, E., Montagner, J.-P., Kiselev, S., Fontaine, F. R., Michon, L., Deplus, C., & Dyment, J. (2019). Large-scale flow of Indian Ocean asthenosphere driven by Réunion plume. *Nature Geoscience*, *12*(12), 1043–1049. https://doi.org/10.1038/s41561-019-0479-3

Beauchamp, W., Allmendinger, R. W., Barazangi, M., Demnati, A., Alji, M. E., & Dahmani, M. (1999). Inversion tectonics and the evolution of the High Atlas Mountains, Morocco, based on a geological-geophysical transect. *Tectonics*, *18*(2), 163–184. https://doi.org/10.1029/1998TC900015

Bezada, M. J., Faccenda, M., & Toomey, D. R. (2016). Representing anisotropic subduction zones with isotropic velocity models: A characterization of the problem and some steps on a possible path forward:

ANISOTROPIC SUBDUCTION, ISOTROPIC MODELS. *Geochemistry, Geophysics, Geosystems*, *17*(8), 3164–3189. https://doi.org/10.1002/2016GC006507

Bezada, M. J., Humphreys, E. D., Davila, J. M., Carbonell, R., Harnafi, M., Palomeras, I., & Levander, A. (2014). Piecewise delamination of Moroccan lithosphere from beneath the Atlas Mountains. *Geochemistry, Geophysics, Geosystems*, *15*, 975–985. https://doi.org/10.1002/2013GC005059

Blackman Donna K. & Kendall J.-Michael. (1997). Sensitivity of teleseismic body waves to mineral texture and melt in the mantle beneath a mid–ocean ridge. *Philosophical Transactions of the Royal Society of London. Series A: Mathematical, Physical and Engineering Sciences*, *355*(1723), 217–231. https://doi.org/10.1098/rsta.1997.0007

Brede, R., Hauptmann, M., & Herbig, H.-G. (1992). Plate tectonics and the intracatonic mountain ranges in Morocco – The Mesozoic – Cenozoic development of the Central High Atlas and the Middle Atlas. *Geologische Rundschau*, *81*. https://doi.org/10.1007/BF01764544

Buontempo, L., Bokelmann, G. H. R., Barruol, G., & Morales, J. (2008). Seismic anisotropy beneath southern Iberia from SKS splitting. *Earth and Planetary Science Letters*, *273*(3), 237–250. https://doi.org/10.1016/j.epsl.2008.06.024

Calvert, A., Sandvol, E., Seber, D., Barazangi, M., Roecker, S., Mourabit, T., Vidal, F., Alguacil, G., & Jabour, N. (2000). Geodynamic evolution of the lithosphere and upper mantle beneath the Alboran region of the western Mediterranean: Constraints from travel time tomography. *Journal of Geophysical Research: Solid Earth*, *105*(B5), 10871–10898. https://doi.org/10.1029/2000JB900024

Chang, S.-J., & Van der Lee, S. (2011). Mantle plumes and associated flow beneath Arabia and East Africa. *Earth and Planetary Science Letters*, *302*(3–4), 448–454. https://doi.org/10.1016/j.epsl.2010.12.050

Christensen, N. I. (1984). The magnitude, symmetry and origin of upper mantle anisotropy based on fabric analyses of ultramafic tectonites. *Geophysical Journal International*, *76*(1), 89–111. https://doi.org/10.1111/j.1365-246X.1984.tb05025.x

Civello, S., & Margheriti, L. (2004). Toroidal mantle flow around the Calabrian slab (Italy) from SKS splitting. *Geophysical Research Letters*, *31*(10). https://doi.org/10.1029/2004GL019607

Conrad, C. P., & Behn, M. D. (2010). Constraints on lithosphere net rotation and asthenospheric viscosity from global mantle flow models and seismic anisotropy. *Geochemistry, Geophysics, Geosystems*, *11*(5). https://doi.org/10.1029/2009GC002970

DePaolo, D. J., & Manga, M. (2003). Deep Origin of Hotspots—The Mantle Plume Model. *Science*, *300*(5621), 920–921. https://doi.org/10.1126/science.1083623

Diaz, J., Gallart, J., Morais, I., Silveira, G., Pedreira, D., Pulgar, J. A., Dias, N. A., Ruiz, M., & González-Cortina, J. M. (2015). From the Bay of Biscay to the High Atlas: Completing the anisotropic characterization of the upper mantle beneath the westernmost Mediterranean region. *Tectonophysics*, *663*, 192–202. https://doi.org/10.1016/j.tecto.2015.03.007

Diaz, J., Gallart, J., Villaseñor, A., Mancilla, F., Pazos, A., Córdoba, D., Pulgar, J. A., Ibarra, P., & Harnafi, M. (2010). Mantle dynamics beneath the Gibraltar Arc (western Mediterranean) from shear-wave splitting measurements on a dense seismic array. *Geophysical Research Letters*, *37*(18). https://doi.org/10.1029/2010GL044201

Duggen, S., Hoernle, K. A., Hauff, F., Klügel, A., Bouabdellah, M., & Thirlwall, M. F. (2009). Flow of Canary mantle plume material through a subcontinental lithospheric corridor beneath Africa to the Mediterranean. *Geology*, *37*(3), 283–286. https://doi.org/10.1130/G25426A.1

Eberhart-Phillips, D., & Mark Henderson, C. (2004). Including anisotropy in 3-D velocity inversion and application to Marlborough, New Zealand. *Geophysical Journal International*, *156*(2), 237–254. https://doi.org/10.1111/j.1365-246X.2003.02044.x

Ebinger, C. J., & Sleep, N. H. (1998). Cenozoic magmatism throughout east Africa resulting from impact of a single plume. *Nature*, *395*(6704), 788–791. https://doi.org/10.1038/27417

Faccenda, M., & Capitanio, F. A. (2012). Development of mantle seismic anisotropy during subduction-induced 3-D flow. *Geophysical Research Letters*, *39*(11). https://doi.org/10.1029/2012GL051988

Faccenna, C., Civetta, L., D'Antonio, M., Funiciello, F., Margheriti, L., & Piromallo, C. (2005). Constraints on mantle circulation around the deforming Clabrian slab. *Geophysical Research Letters*, *32*. https://doi.org/10.1029/2004GL021874

Fouch, M. J., & Rondenay, S. (2006). Seismic anisotropy beneath stable continental interiors. *Physics of the Earth and Planetary Interiors*, *158*(2), 292–320. https://doi.org/10.1016/j.pepi.2006.03.024

French, S. W., & Romanowicz, B. (2015). Broad plumes rooted at the base of the Earth's mantle beneath major hotspots. *Nature*, *525*(7567), 95–99. https://doi.org/10.1038/nature14876

Frizon de Lamotte, D., Bezar, B. S., Bracène, R., & Mercier, E. (2000). The two main steps of the Atlas building and geodynamics of the western Mediterranean. *Tectonics*, *19*(4), 740–761. https://doi.org/10.1029/2000TC900003

Fullea, J., Fernàndez, M., Afonso, J. C., Vergés, J., & Zeyen, H. (2010). The structure and evolution of the lithosphere–asthenosphere boundary beneath the Atlantic–Mediterranean Transition Region. *Lithos*, *120*(1–2), 74–95. https://doi.org/10.1016/j.lithos.2010.03.003

Füri, E., Hilton, D. R., Murton, B. J., Hémond, C., Dyment, J., & Day, J. M. D. (2011). Helium isotope variations between Réunion Island and the Central Indian Ridge (17°–21°S): New evidence for ridge–hot spot interaction. *Journal of Geophysical Research: Solid Earth*, *116*(B2). https://doi.org/10.1029/2010JB007609

Gomez, F., Allmendinger, R., Barazangi, M., Er-Raji, A., & Dahmani, M. (1998). Crustal shortening and vertical strain partitioning in the Middle Atlas Mountains of Morocco. *Tectonics*, *17*(4), 520–533. https://doi.org/10.1029/98TC01439

Hammond, W. C., & Toomey, D. R. (2003). Seismic velocity anisotropy and heterogeneity beneath the Mantle Electromagnetic and Tomography Experiment (MELT) region of the East Pacific Rise from analysis of *P* and *S* body waves: EPR SEISMIC VELOCITY AND ANISOTROPY. *Journal of Geophysical Research: Solid Earth*, *108*(B4). https://doi.org/10.1029/2002JB001789

Hansen, S. E., Nyblade, A. A., & Benoit, M. H. (2012). Mantle structure beneath Africa and Arabia from adaptively parameterized P-wave tomography: Implications for the origin of Cenozoic Afro-Arabian tectonism. *Earth and Planetary Science Letters*, *319–320*, 23–34. https://doi.org/10.1016/j.epsl.2011.12.023

Hirschmann, M. M. (2000). Mantle solidus: Experimental constraints and the effects of peridotite composition: MANTLE SOLIDUS. *Geochemistry, Geophysics, Geosystems*, *1*(10), n/a-n/a. https://doi.org/10.1029/2000GC000070

Hirth, G., & Kohlstedt, D. (2003). Rheology of the upper mantle and the mantle wedge: A view from the experimentalists. In J. Eiler (Ed.), *Geophysical Monograph Series* (Vol. 138, pp. 83–105). American Geophysical Union. https://doi.org/10.1029/138GM06

Hu, J., Faccenda, M., & Liu, L. (2017). Subduction-controlled mantle flow and seismic anisotropy in South America. *Earth and Planetary Science Letters*, *470*, 13–24. https://doi.org/10.1016/j.epsl.2017.04.027

Humphreys, E. D., Dueker, K. G., Schutt, D. L., & Smith, R. B. (2000). Beneath Yellowstone: Evaluating Plume and Nonplume Models Using Teleseismic Images of the Upper Mantle. *GSA TODAY*, 7.

Ishise, M., & Oda, H. (2005). Three-dimensional structure of P-wave anisotropy beneath the Tohoku district, northeast Japan. *Journal of Geophysical Research: Solid Earth*, *110*(B7). https://doi.org/10.1029/2004JB003599

Ismaïl, W. B., & Mainprice, D. (1998). An olivine fabric database: An overview of upper mantle fabrics and seismic anisotropy. *Tectonophysics*, *296*(1–2), 145–157. https://doi.org/10.1016/S0040-1951(98)00141-3

Ito, G., Dunn, R., Li, A., Wolfe, C. J., Gallego, A., & Fu, Y. (2014). Seismic anisotropy and shear wave splitting associated with mantle plume-plate interaction. *Journal of Geophysical Research: Solid Earth*, *119*(6), 4923–4937. https://doi.org/10.1002/2013JB010735

Kaislaniemi, L., & van Hunen, J. (2014). Dynamics of lithospheric thinning and mantle melting by edge-driven convection: Application to Moroccan Atlas mountains. *Geochemistry, Geophysics, Geosystems*, *15*(8), 3175–3189. https://doi.org/10.1002/2014GC005414

Kaminski, É., & Ribe, N. M. (2002). Timescales for the evolution of seismic anisotropy in mantle flow. *Geochemistry, Geophysics, Geosystems*, *3*(8), 1–17. https://doi.org/10.1029/2001GC000222

Katz, R. F., Spiegelman, M., & Langmuir, C. H. (2003). A new parameterization of hydrous mantle melting. *Geochemistry, Geophysics, Geosystems*, *4*(9). https://doi.org/10.1029/2002GC000433

Kern, H. (1993). P- and S-wave anisotropy and shear-wave splitting at pressure and temperature in possible mantle rocks and their relation to the rock fabric. *Physics of the Earth and Planetary Interiors*, *78*(3), 245–256. https://doi.org/10.1016/0031-9201(93)90159-7

Lee, H., Bezada, M. J., & Faccenda, M. (2021). Can sub-slab low-velocity anomalies be an artifact caused by anisotropy? A case study from the Alboran slab area in the western Mediterranean. *Tectonophysics*, 229080. https://doi.org/10.1016/j.tecto.2021.229080

Lloyd, S. M., & Van der Lee, S. (2008). Influence of observed mantle anisotropy on isotropic tomographic models. *Geochemistry, Geophysics, Geosystems*, *9*(7). https://doi.org/10.1029/2008GC001997

Long, M. D., & Becker, T. W. (2010). Mantle dynamics and seismic anisotropy. *Earth and Planetary Science Letters*, *297*(3–4), 341–354. https://doi.org/10.1016/j.epsl.2010.06.036

Long, M. D., & Silver, P. G. (2008). The Subduction Zone Flow Field from Seismic Anisotropy: A Global View. *Science*, *319*(5861), 315–318. https://doi.org/10.1126/science.1150809

Lustrino, M., & Wilson, M. (2007). The circum-Mediterranean anorogenic Cenozoic igneous province. *Earth-Science Reviews*, *81*(1–2), 1–65. https://doi.org/10.1016/j.earscirev.2006.09.002

Miller, M. S., Allam, A. A., Becker, T. W., Di Leo, J. F., & Wookey, J. (2013). Constraints on the tectonic evolution of the westernmost Mediterranean and northwestern Africa from shear wave splitting analysis. *Earth and Planetary Science Letters*, *375*, 234–243. https://doi.org/10.1016/j.epsl.2013.05.036

Miller, M. S., & Becker, T. W. (2014). Reactivated lithospheric-scale discontinuities localize dynamic uplift of the Moroccan Atlas Mountains. *Geology*, *42*(1), 35–38. https://doi.org/10.1130/G34959.1

Miller, M. S., O'Driscoll, L. J., Butcher, A. J., & Thomas, C. (2015). Imaging Canary Island hotspot material beneath the lithosphere of Morocco and southern Spain. *Earth and Planetary Science Letters*, *431*, 186–194. https://doi.org/10.1016/j.epsl.2015.09.026

Missenard, Y., & Cadoux, A. (2012). Can Moroccan Atlas lithospheric thinning and volcanism be induced by Edge-Driven Convection? *Terra Nova*, *24*(1), 27–33. https://doi.org/10.1111/j.1365-3121.2011.01033.x

Missenard, Y., Zeyen, H., Frizon de Lamotte, D., Leturmy, P., Petit, C., Sébrier, M., & Saddiqi, O. (2006). Crustal versus asthenospheric origin of relief of the Atlas Mountains of Morocco: ORIGIN OF RELIEF IN ATLAS MOUNTAINS. *Journal of Geophysical Research: Solid Earth*, *111*(B3), n/a-n/a. https://doi.org/10.1029/2005JB003708

Montelli, R., Nolet, G., Dahlen, F. A., & Masters, G. (2006). A catalogue of deep mantle plumes: New results from finite-frequency tomography. *Geochemistry, Geophysics, Geosystems*, *7*(11). https://doi.org/10.1029/2006GC001248

Morgan, W. J. (1971). Convection Plumes in the Lower Mantle. *Nature*, *230*(5288), 42–43. https://doi.org/10.1038/230042a0

Morgan, W. J. (1978). Rodriguez, Darwin, Amsterdam, ..., A second type of Hotspot Island. *Journal of Geophysical Research: Solid Earth*, *83*(B11), 5355–5360. https://doi.org/10.1029/JB083iB11p05355

Nolet, G., Allen, R., & Zhao, D. (2007). Mantle plume tomography. *Chemical Geology*, *241*(3–4), 248–263. https://doi.org/10.1016/j.chemgeo.2007.01.022

Palomeras, I., Thurner, S., Levander, A., Liu, K., Villasenor, A., Carbonell, R., & Harnafi, M. (2014). Finite-frequency Rayleigh wave tomography of the western Mediterranean: Mapping its lithospheric structure. *Geochemistry, Geophysics, Geosystems*, *15*(1), 140–160. https://doi.org/10.1002/2013GC004861

Piqué, A., Tricart, P., Guiraud, R., Laville, E., Bouaziz, S., Amrhar, M., & Ait Ouali, R. (2002). The Mesozoic–Cenozoic Atlas belt (North Africa): An overview. *Geodinamica Acta*, *15*(3), 185–208. https://doi.org/10.1016/S0985-3111(02)01088-4

Portner, D. E., Beck, S., Zandt, G., & Scire, A. (2017). The nature of subslab slow velocity anomalies beneath South America: Subslab Slow Velocity Anomalies. *Geophysical Research Letters*, *44*(10), 4747–4755. https://doi.org/10.1002/2017GL073106

Ramdani, F. (1998). Geodynamic implications of intermediate-depth earthquakes and volcanism in the intraplate Atlas mountains (Morocco). *Physics of the Earth and Planetary Interiors*, *108*, 245–260. https://doi.org/10.1016/S0031-9201(98)00106-X

Ribe, N. M., & Christensen, U. R. (1994). Three-dimensional modeling of plume-lithosphere interaction. *Journal of Geophysical Research: Solid Earth*, *99*(B1), 669–682. https://doi.org/10.1029/93JB02386

Ribe, N. M., & Christensen, U. R. (1999). The dynamical origin of Hawaiian volcanism. *Earth and Planetary Science Letters*, *171*(4), 517–531. https://doi.org/10.1016/S0012-821X(99)00179-X

Richards, M. A., & Griffiths, R. W. (1988). Deflection of plumes by mantle shear flow: Experimental results and a simple theory. *Geophysical Journal International*, *94*(3), 367–376. https://doi.org/10.1111/j.1365-246X.1988.tb02260.x

Ritter, J. R. R., Jordan, M., Christensen, U. R., & Achauer, U. (2001). A mantle plume below the Eifel volcanic fields, Germany. *Earth and Planetary Science Letters*, *186*(1), 7–14. https://doi.org/10.1016/S0012-821X(01)00226-6

Russo, R. M., & Silver, P. G. (1994). Trench-Parallel Flow Beneath the Nazca Plate from Seismic Anisotropy. *Science*, *263*(5150), 1105–1111. https://doi.org/10.1126/science.263.5150.1105

Sandvol, E., Seber, D., Calvert, A., & Barazangi, M. (1998). Grid search modeling of receiver functions: Implications for crustal structure in the Middle East and North Africa. *Journal of Geophysical Research: Solid Earth*, *103*(B11), 26899–26917. https://doi.org/10.1029/98JB02238

Seber, D., Barazangi, M., Tadili, B. A., Ramdani, M., Ibenbrahim, A., & Sari, D. B. (1996). Three-dimensional upper mantle structure beneath the intraplate Atlas and interplate Rif mountains of Morocco. *Journal of Geophysical Research: Solid Earth*, *101*(B2), 3125–3138. https://doi.org/10.1029/95JB03112

Silver, P. G. (1996). SEISMIC ANISOTROPY BENEATH THE CONTINENTS: Probing the Depths of Geology. *Annual Review of Earth and Planetary Sciences*, *24*(1), 385–432. https://doi.org/10.1146/annurev.earth.24.1.385

Sleep, N. H. (1990). Hotspots and mantle plumes: Some phenomenology. *Journal of Geophysical Research*, *95*(B5), 6715. https://doi.org/10.1029/JB095iB05p06715

Sleep, N. H. (2008). Channeling at the base of the lithosphere during the lateral flow of plume material beneath flow line hot spots. *Geochemistry, Geophysics, Geosystems*, *9*(8). https://doi.org/10.1029/2008GC002090

Sun, D., Miller, M. S., Holt, A. F., & Becker, T. W. (2014). Hot upwelling conduit beneath the Atlas Mountains, Morocco. *Geophysical Research Letters*, *41*(22), 8037–8044. https://doi.org/10.1002/2014GL061884

Teixell, A., Arboleya, M.-L., Julivert, M., & Charroud, M. (2003). Tectonic shortening and topography in the central High Atlas (Morocco). *Tectonics*, *22*(5). https://doi.org/10.1029/2002tc001460

Teixell, A., Ayarza, P., Zeyen, H., Fernàndez, M., & Arboleya, M.-L. (2005). Effects of mantle upwelling in a compressional setting: The Atlas Mountains of Morocco. *Terra Nova*, *17*(5), 456–461. https://doi.org/10.1111/j.1365-3121.2005.00633.x

Teixell, A., Bertotti, G., de Lamotte, D. F., & Charroud, M. (2009). The geology of vertical movements of the lithosphere: An overview. *Tectonophysics*, *475*(1), 1–8. https://doi.org/10.1016/j.tecto.2009.08.018

Thoraval, C., Tommasi, A., & Doin, M.-P. (2006). Plume-lithosphere interaction beneath a fast moving plate: PLUME-LITHOSPHERE INTERACTION. *Geophysical Research Letters*, *33*(1), n/a-n/a. https://doi.org/10.1029/2005GL024047

Timoulali, Y., Bouiflane, M., Bouskri, G., Azguet, R., & El Fellah, Y. (2019). Lithosphere structures dynamics in the central High Atlas (Morocco) by seismic tomography and gravimetric data. *Geodesy and Geodynamics*, *10*(3), 241–255. https://doi.org/10.1016/j.geog.2019.01.005

Timoulali, Y., Nacer, J., Youssef, H., & Mimoun, C. (2015). Lithospheric structure in NW of Africa: Case of the Moroccan Atlas Mountains. *Geodesy and Geodynamics*, *6*(6), 397–408. https://doi.org/10.1016/j.geog.2015.12.003

Tommasi, A., Tikoff, B., & Vauchez, A. (1999). Upper mantle tectonics: Three-dimensional deformation, olivine crystallographic fabrics and seismic properties. *Earth and Planetary Science Letters*, *168*(1), 173–186. https://doi.org/10.1016/S0012-821X(99)00046-1

Toomey, D. R., Solomon, S. C., & Purdy, G. M. (1994). Tomographic imaging of the shallow crustal structure of the East Pacific Rise at 9°30′N. *Journal of Geophysical Research: Solid Earth*, *99*(B12), 24135–24157. https://doi.org/10.1029/94JB01942

VanDecar, J. C., & Crosson, R. S. (1990). Determination of teleseismic relative phase arrival times using multi-channel cross-correlation and least squares. *Bulletin of the Seismological Society of America*, *80*(1), 150–169.

Walker, A. M., & Wookey, J. (2012). MSAT—A new toolkit for the analysis of elastic and seismic anisotropy. *Computers & Geosciences*, *49*, 81–90. https://doi.org/10.1016/j.cageo.2012.05.031

Wilson, J. T. (1963). A Possible origin of the Hawaiian Islands. *Canadian Journal of Earth Sciences*, *51*, 863–870.

Wu, H., & Lees, J. M. (1999). *Cartesian parametrization of anisotropic traveltime tomography*. https://doi.org/10.1046/J.1365-246X.1999.00778.X

Zeyen, H., Ayarza, P., Fernàndez, M., & Rimi, A. (2005). Lithospheric structure under the western African-European plate boundary: A transect across the Atlas Mountains and the Gulf of Cadiz. *Tectonics*, *24*(2). https://doi.org/10.1029/2004TC001639

Zhao, D. (2007). Seismic images under 60 hotspots: Search for mantle plumes. *Gondwana Research*, *12*(4), 335–355. https://doi.org/10.1016/j.gr.2007.03.001

(a)

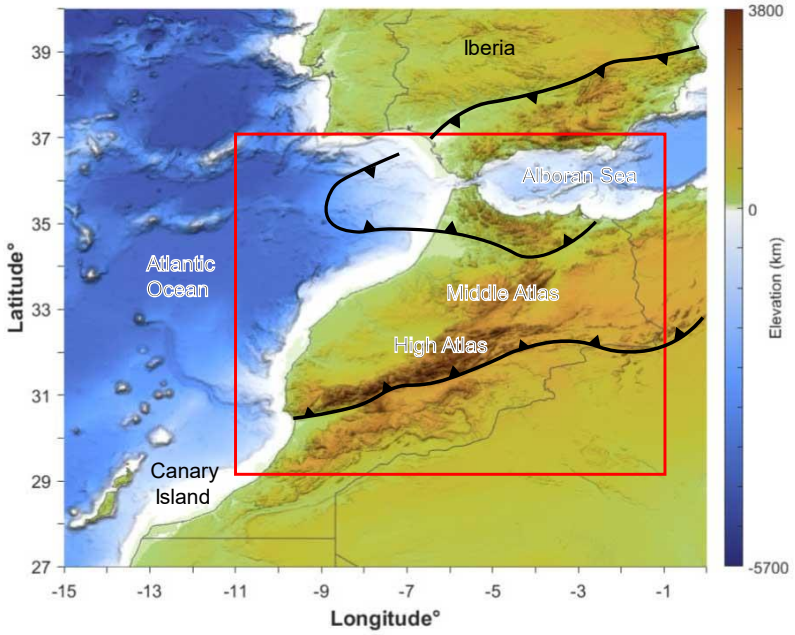
Iberia
Alboran Sea
Atlantic Ocean
Middle Atlas
High Atlas
Canary Island
Latitude°
Longitude°
Elevation (km)
3800
0
-5700
39
37
35
33
31
29
27
-15
-13
-11
-9
-7
-5
-3
-1

(b)

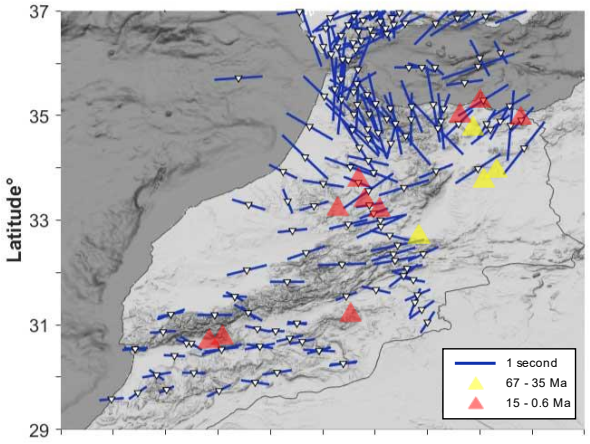
Latitude°
37
35
33
31
29
1 second
67 - 35 Ma
15 - 0.6 Ma

(c)

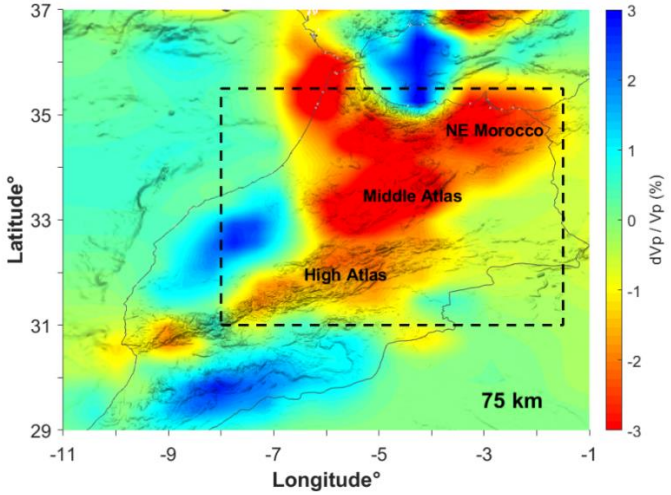
NE Morocco
Middle Atlas
High Atlas
75 km
Latitude°
Longitude°
dVp / Vp (%)
37
35
33
31
29
-11
-9
-7
-5
-3
-1
3
2
1
0
-1
-2
-3

Figure 1. (a) The physiographic features of the regional map. The red rectangle shows the study area. Black lines with sawteeth show the location of the thrust fault. The solid-red box presents the area shown in Figures 1b and 1c. (b) The observation of shear wave splitting (SWS) (Diaz et al., 2010; Miller et al., 2013) at stations (white triangle). The length of the blue bar indicates the SWS time while the orientation represents the fast polarization direction (FPD). The yellow and red triangles show the approximated location of volcanoes that erupted during 67 – 35 Ma and 15 – 0.6 Ma, respectively (Teixell et al., 2005). (c) The depth slice of isotropic P-wave tomography at 75 km for the study region, showing extensive low-velocity anomalies across the Moroccan Atlas and NE Morocco. The black-dashed box indicates the region used in the analysis of this study.

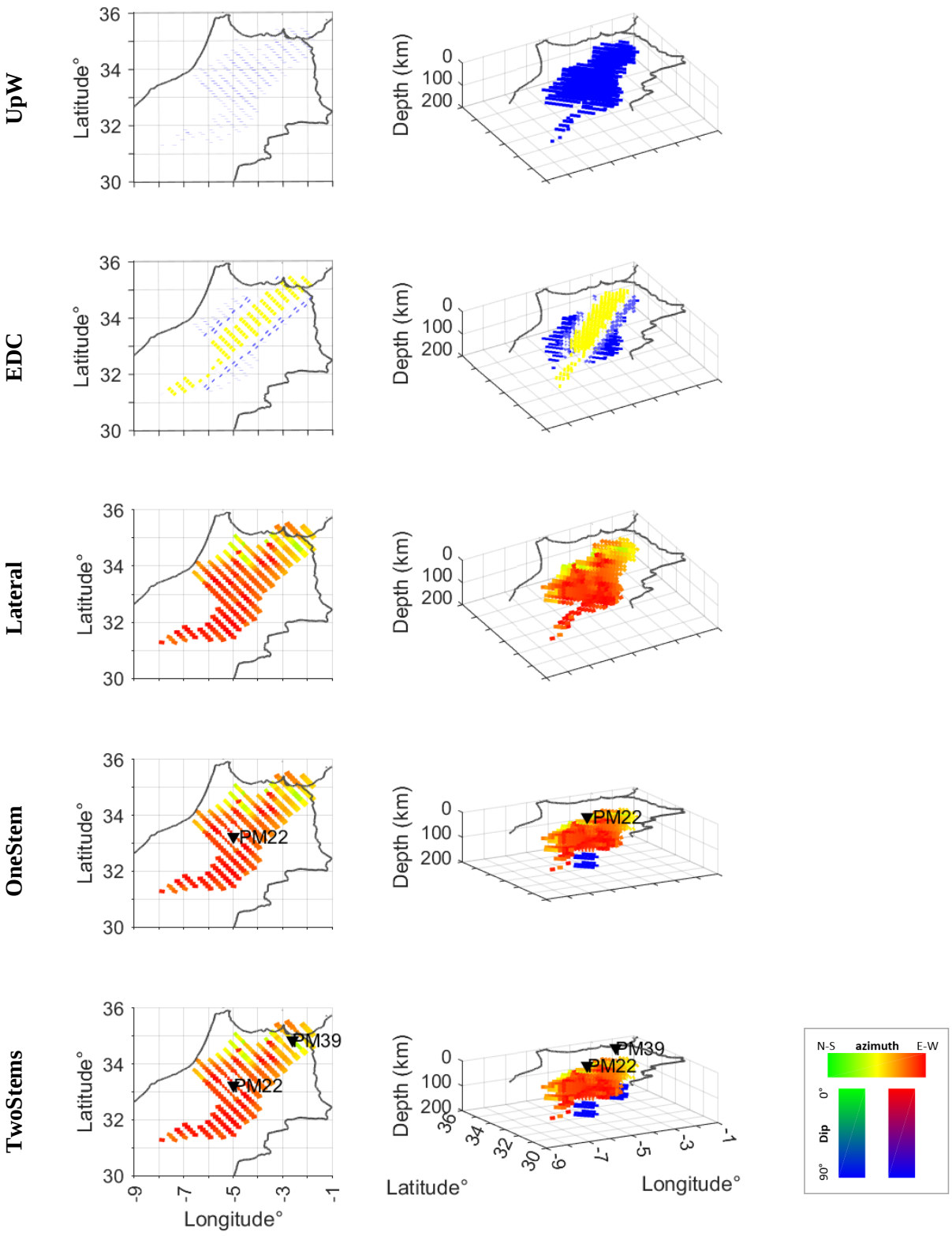
UpW
EDC
Lateral
OneStem
TwoStems
Latitude°
Depth (km)
Longitude°
PM22
PM39
N-S
azimuth
E-W
Dip
0°
90°

Figure 2. The five anisotropy models used in this study. Each model is placed below the High Atlas, the Middle Atlas, and NE Morroco at 60 – 160 km depth except for OneStem and TwoStems that the stem portions extend to 200 km depth. The shape and depth distribution are taken from the distribution of low-velocity anomalies in the isotropic tomography that are ≤ -2.0% of dVp/Vp (Figure S2). The length of the bar represents the field of anisotropy. The orientation of the bar represents the seismically fast direction (SFD) of the anisotropy model and it is colored by azimuth and dip. Figure S3 shows zoom-in views.

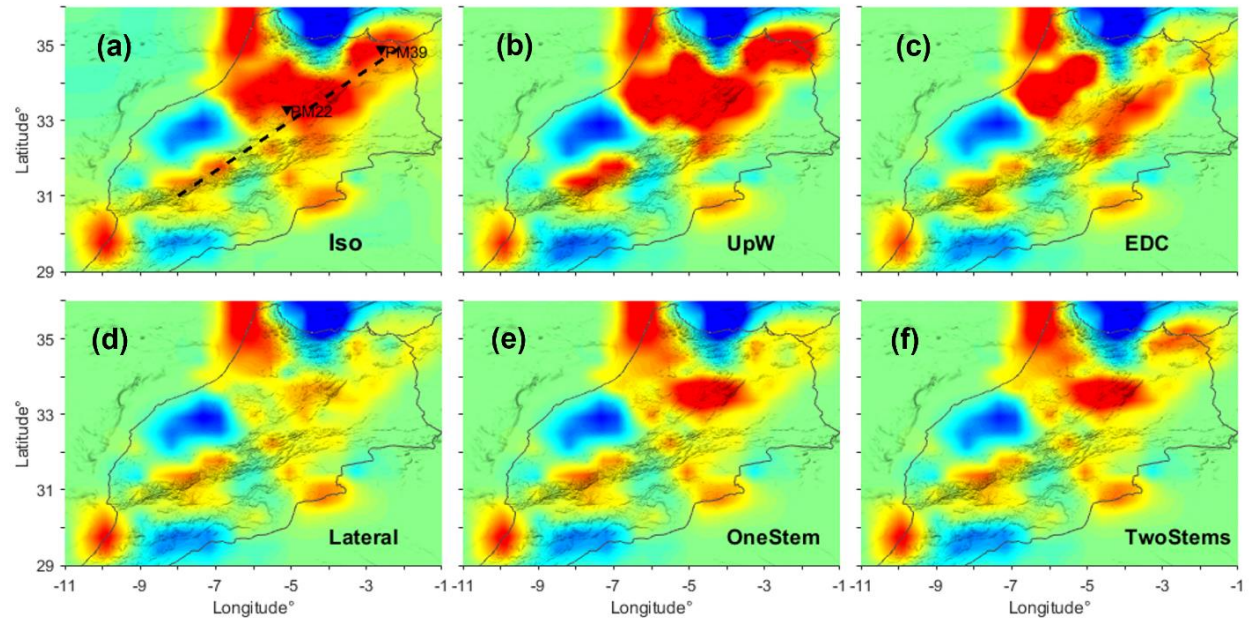
(a)
(b)
(c)
(d)
(e)
(f)
PM39
PM22
Iso
UpW
EDC
Lateral
OneStem
TwoStems
Latitude°
Longitude°
35
33
31
29
-11
-9
-7
-5
-3
-1

671

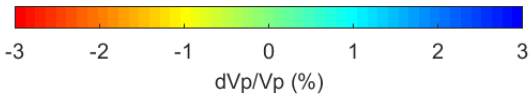
-3
-2
-1
0
1
2
3
dVp/Vp (%)

672

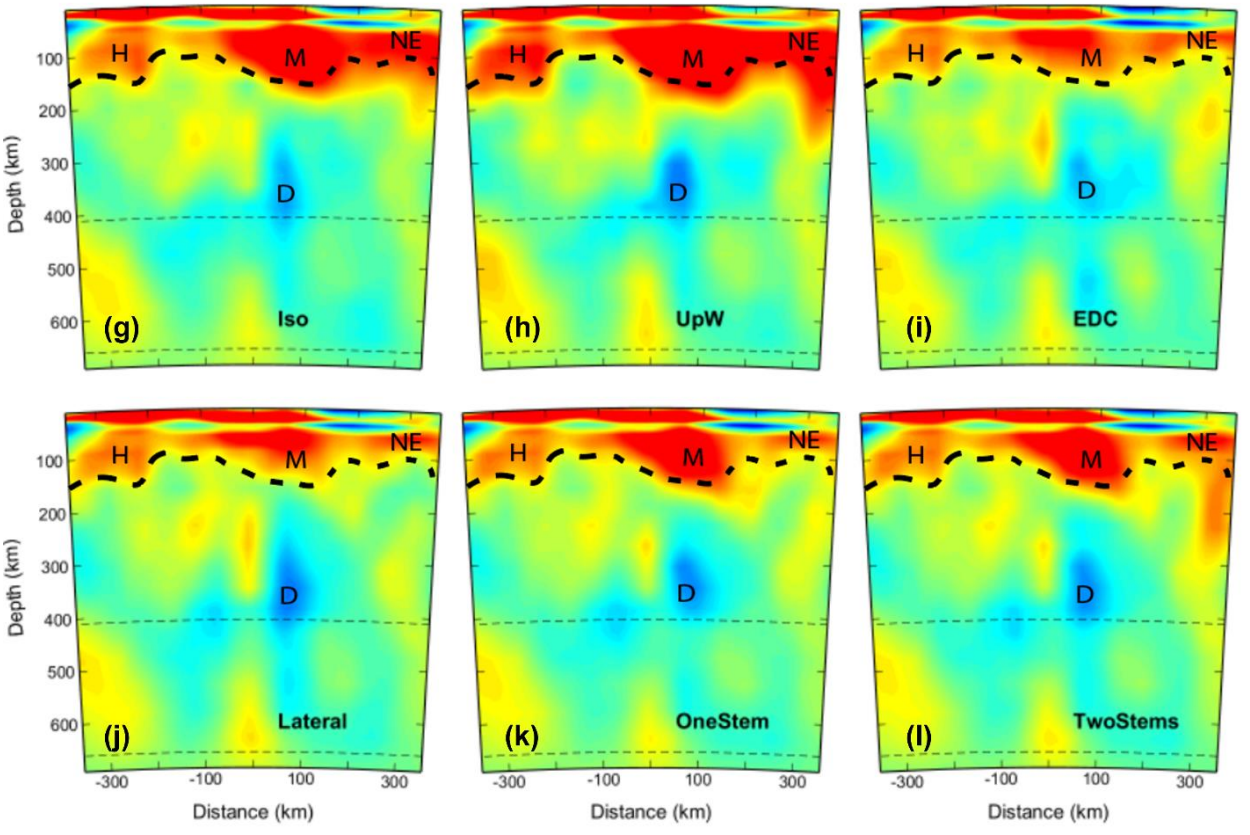
(g)
(h)
(i)
(j)
(k)
(l)
Iso
UpW
EDC
Lateral
OneStem
TwoStems
H
M
NE
D
Depth (km)
100
200
300
400
500
600
-300
-100
100
300
Distance (km)

673

Figure 3. (a) – (f) The tomographic slices at 125 km depth of the isotropy and anisotropy models. The black dashed line in (a) presents the cross-sectional line ([31°N, 8°W] to [35°N, 2°W]) for (g) – (l), which show cross-sectional views of each model. The black thick-dashed lines in (g) – (l) is the base of low-velocity anomalies observed from model Lateral (k). The regions denoted by 'H', 'M', and 'NE' in (g) – (l) are High Atlas, Middle Atlas, and NE Morocco, respectively.

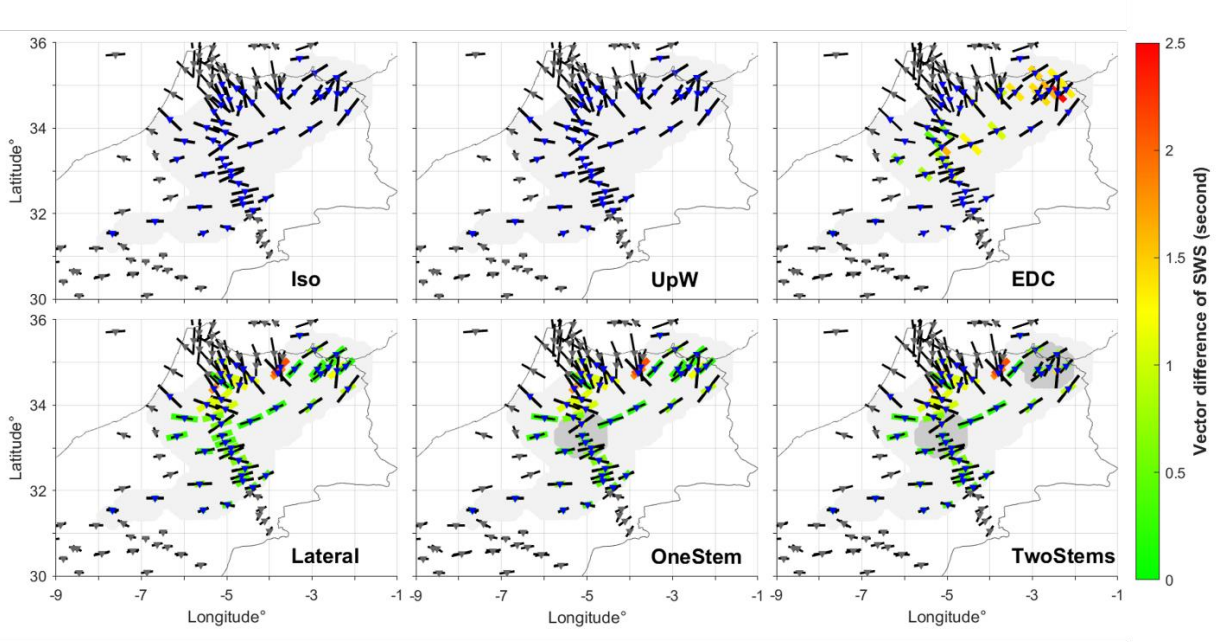

680

681 **Figure 4.** Predicted SWS by MSAT. The light-gray shaded area represents the spatial distribution of
682 anisotropy models while the darker-gray circles in OneStem and TwoStems represent the locations of the
683 stems.

684

685

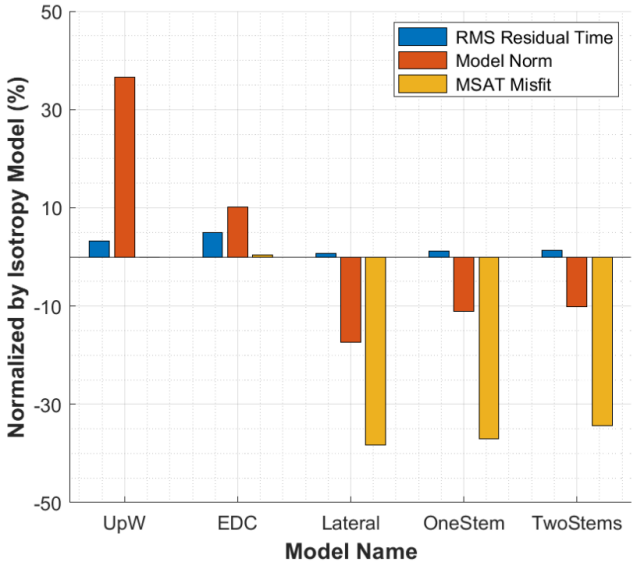

686

687 **Figure 5.** Bar graphs that show the changes in RMS residual (blue), model norm (orange), and MSAT
688 misfit representing SWS (yellow) in % compared to the isotropy model within the black-dashed-line box
689 in Figure 1c at 60 – 200 km depth.

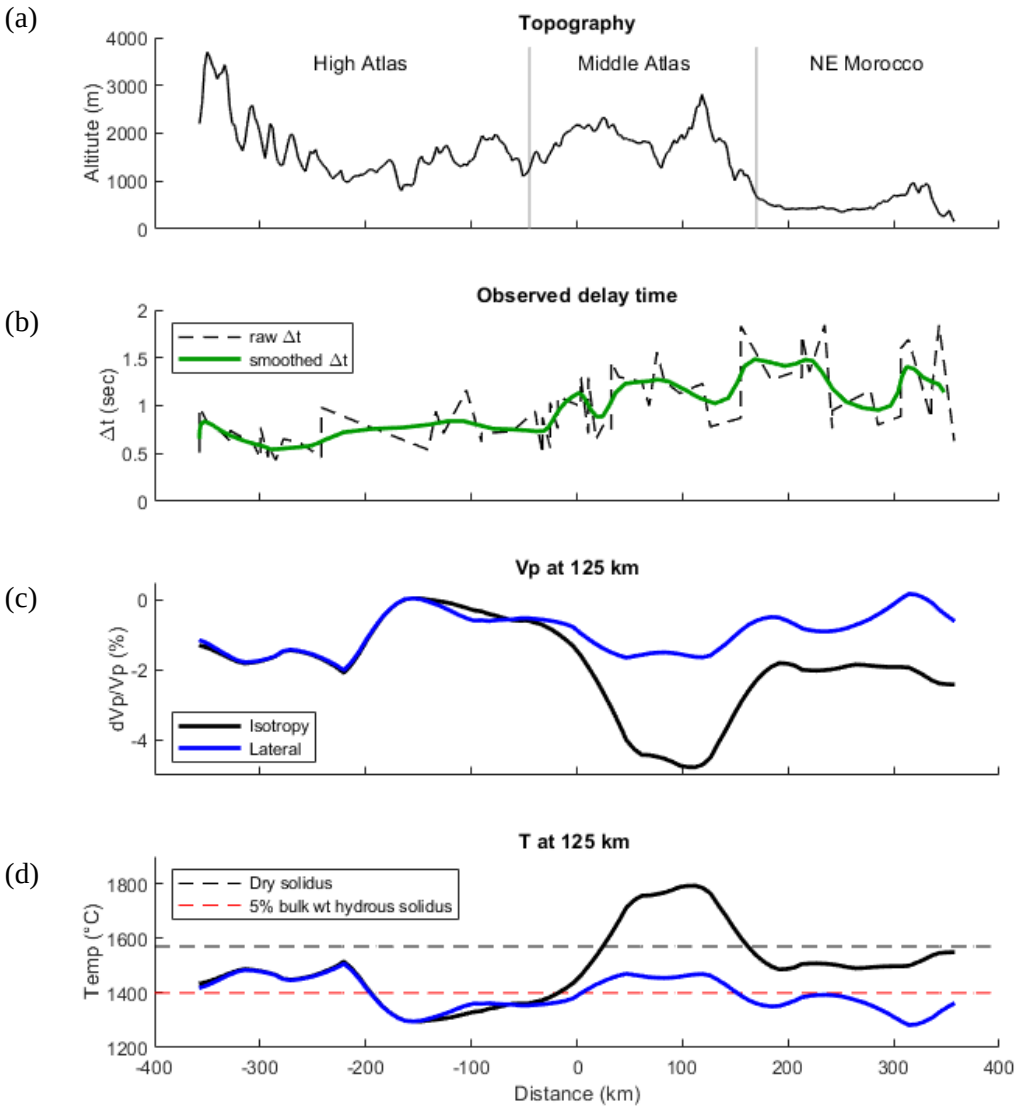

690

691 **Figure 6.** The change of (a) topography; (b) observed delay time from SWS (Diaz et al., 2010; Miller et
692 al., 2013); (c) change in dVp/Vp at 125 km depth for the isotropy tomography (black line) and anisotropy
693 tomography including model Lateral (blue line); (d) estimated temperature from the isotropy tomography
694 (black line) and anisotropy tomography (blue line) based on the temperature derivatives of Vp
695 (Cammarano, 2013) at 125 km (4 GPa) along with the black solid line in Figure 3a ([31°N, 8°W] to
696 [35°N, 2°W]). The dry solidus is at 1570°C (Hirschmann, 2000), and the 5-bulk-weight-% hydrous
697 solidus is at 1400°C (Katz et al., 2003).
698

699

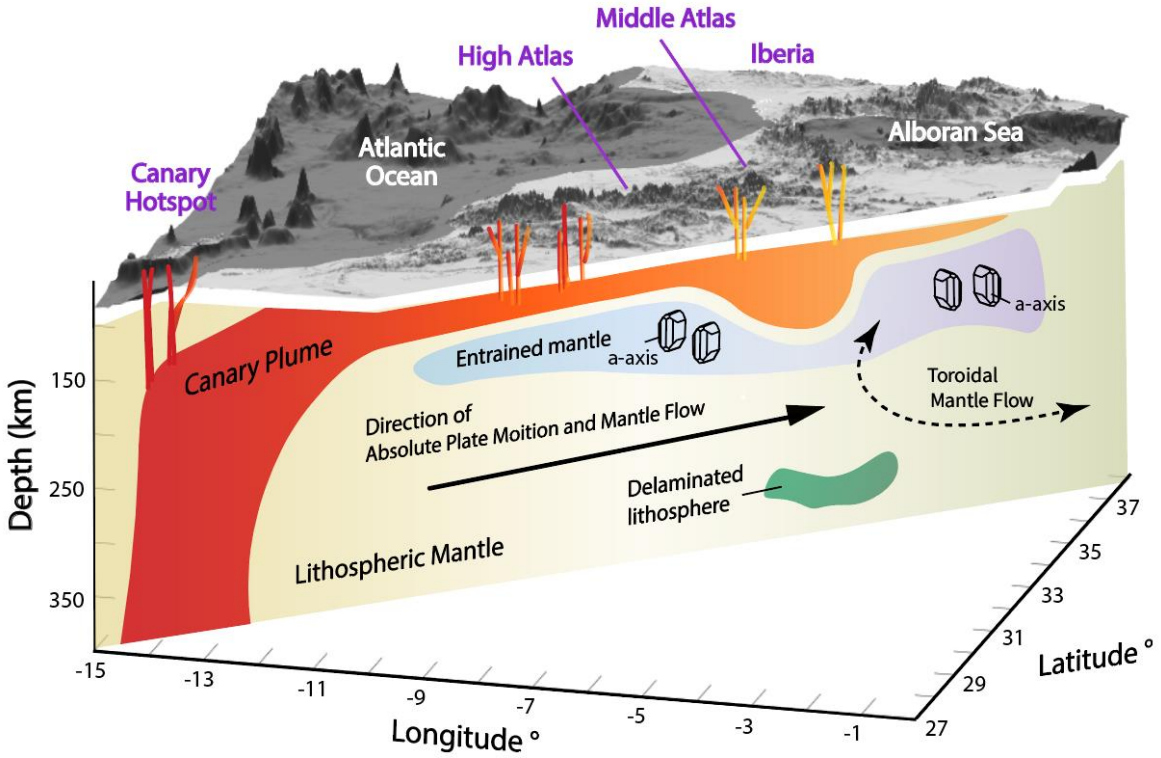

Figure 7. A schematic view for the lateral travel of the Canary plume. It shows that the lateral travel of the Canary Plume has entrained the mantle below and may have developed seismic anisotropy consequently beneath the Atlas Mountains while the toroidal mantle flow generated by the rollback of the Alboran slab may contribute to the observed seismic anisotropy by SWS. The scale is not absolute.